REPORT NO.
ATN-64(9227)-2

General Research

Confined Vortex Flows with Boundary-Layer Interaction

20 FEBRUARY 1964

Prepared by M. L. ROSENZWEIG, W. S. LEWELLEN, and D. H. ROSS
Aerodynamics and Propulsion Research Laboratory

Prepared for VICE PRESIDENT and GENERAL MANAGER
LABORATORY OPERATIONS

AEROSPACE CORPORATION

Report No.
ATN-64(9227)-2

GENERAL RESEARCH

Confined Vortex Flows With Boundary-Layer Interaction

Prepared by

M. L. Rosenzweig, W. S. Lewellen, and D. H. Ross
Aerodynamics and Propulsion Research Laboratory

AEROSPACE CORPORATION
El Segundo, California

20 February 1964

Prepared for

VICE PRESIDENT AND GENERAL MANAGER
LABORATORY OPERATIONS

ABSTRACT

Axisymmetric flow of an incompressible fluid in a right-cylindrical vortex tube bounded by planar end walls is considered. The mutual interaction of the primary vortex flow field and the end-wall boundary layers is studied by relating the stream function and circulation in these regions. An interaction parameter is defined which determines the magnitude of the influence of the boundary layers on the circulation and mass-flow distributions in the primary flow. These distributions are obtained numerically, primarily as functions of the interaction parameter and the Reynolds number based on the radial flow. Experimental results are interpreted in the light of this theory, and it is concluded that substantial turbulence levels (though somewhat less than estimates made without consideration of boundary layer effects) must be assumed to explain the experimental results.

CONTENTS

FIGURES

FIGURES (Continued)

NOMENCLATURE

A	=	Boundary-layer interaction parameter defined in Eq. (17)
c	=	Coefficient of friction
F	=	Dimensionless part of the stream function which is independent of z
f	=	Dimensionless part of the stream function which is linear with z
ℓ	=	Length of the vortex chamber
p	=	Pressure
Q	=	Volume flow per unit length
Q_{BL}	=	Volume flow in the end-wall boundary layer
Re_r	=	Radial Reynolds number = $\rho ur/\mu$
Re_r^*	=	"Effective" turbulent radial Reynolds number
Re_t	=	Tangential Reynolds number = $\rho vr/\mu$
r	=	Radial coordinate
u	=	Radial velocity, positive outward
v	=	Tangential velocity
w	=	Axial velocity
z	=	Axial coordinate
α	=	Velocity-profile shape parameter in the boundary layer
Γ	=	Circulation - vr
δ	=	End-wall boundary-layer thickness
ϵ	=	Dimensionless parameter defined in Eq. (5)
η	=	Dimensionless radial coordinate squared

NOMENCLATURE (Continued)

μ	=	Viscosity
ν	=	Kinematic Viscosity
ξ	=	Dimensionless axial coordinate
ρ	=	Density
ψ	=	Stream function defined in Eq. (7)

Subscripts

0	=	Denotes value at outer edge of the vortex tube
e	=	Denotes value at the edge of the exhaust hole
m	=	Denotes minimum value

I. INTRODUCTION

Vortex tubes of one form or another have been of interest to fluid dynamicists for some time. Applications such as the Ranque-Hilsch tube, cyclone separator, and, more recently, the MHD vortex power generator[1] and gaseous-core nuclear rocket,[2] have provided the stimulus for research in this field. Analytical and experimental investigations of confined vortex flows have been numerous. The theoretical treatments have been concerned with the main body of rotating fluid and have, for the most part, been restricted to one-dimensional flow models (i.e., tangential and radial velocities being functions of radius only). Donaldson[3] examined the full Navier-Stokes equations under these assumptions and found a family of exact solutions. These exact solutions are not readily applicable to the flow in an actual vortex tube, however, because of their inability to satisfy boundary conditions imposed by the end walls and exhaust-hole geometry. Others[4,5] have developed approximate theories in which the radial distributions of axial velocity are specified (rather arbitrarily) in order to satisfy conditions imposed by the exhaust ports. A notable exception is a study by Anderson[6] in which the laminar end-wall boundary-layer interaction problem was first treated.

Lewellen[7] has reviewed these studies and has clarified the mathematical foundation of the approximate solutions. In particular he has shown that under certain circumstances (which are usually met experimentally), the one-dimensional hypothesis can yield a valid first approximation to the solution. In regions where this is the case, the axial velocity distribution is determined to the same degree of exactness by its boundary values. In an actual vortex tube, these are determined by the boundary layers on the end walls and by the location and geometry of the exit port (or ports), as mentioned above. Solutions based on arbitrarily specified axial velocity distributions have been

reasonably successful in predicting the qualitative behavior of the measured tangential velocity distributions, numerical discrepancies being attributed usually to turbulence in the flow field.[4, 8, 9]

The boundary layers which are formed on the end walls of the vortex chamber have been studied previously without regard to their effect on the primary vortex flow which drives them. Boundary-layer growth on a finite disc under the influence of a vortex-like outer flow has been studied, originally by Taylor,[10] and more recently by Mack[11], King,[12] Weber,[13] Rott,[14] and others. These studies, in which the external velocity distributions were specified functions of the radial coordinate, have demonstrated that such boundary layers are capable of transporting large quantities of fluid radially inward. This radial flow is coupled through the continuity equation to an axial flow, so that in fact it is the boundary-layer flow which determines, for the most part, the axial velocity distribution in a vortex tube.

For a fixed total flow through the tube, diversion of fluid into the boundary layers reduces the radial flow through the main body of the vortex and tends to weaken the vortex strength, or circulation. In an actual vortex tube (such as pictured in Fig. 1), however, the boundary layers must at some point discharge their contents. If this process is accomplished in such a way as to return the boundary-layer fluid to the main flow before it has lost much of its angular momentum and before it is passed axially out of the tube, then (as is described in this paper) it is possible to maintain a near-constant circulation distribution in the vortex. This point is illustrated in Fig. 2: fluid following paths 1 and 2 will contribute to the support of the circulation distribution, while that following paths 3 and 4 will not.

Mass flow may be caused to leave the boundary layer for two reasons. First, the boundary-layer theory itself indicates mass ejection when the external circulation distribution decreases with decreasing radius.[12] Second, certain discontinuities in the wall geometry, such as a circular step or the sharp edge of an exhaust orifice (i.e., regions where boundary-layer theory is not locally applicable), can also induce mass ejection. Experimental

evidence of such boundary-layer mass ejection is plentiful;[16, 17, 18] several examples are given in Figs. 3 and 4. Figure 3 shows boundary-layer mass ejection in the vicinity of the exhaust-hole radius, resulting, most likely, from both mechanisms. Figure 4 illustrates the effect of a circular step in the end wall at approximately mid-radius. Mass ejection is again observed.

The full three-dimensional flow pattern in a vortex tube is thus the result of a complicated interaction between the primary vortex flow and the end-wall boundary layers. The purpose of the present paper is to study this interaction theoretically in order to demonstrate the unusual mutual influences which are exerted by the primary and secondary flows in right-cylindrical vortex tubes of the type illustrated in Fig. 1. The results are compared with experiments and, as a corollary, certain observations are made concerning turbulence levels in confined vortex flows.

II. DESCRIPTION OF FLOW MODEL

An incompressible, constant viscosity fluid is assumed. For the purposes of the analysis the flow is considered divisible into three regions, as indicated in Fig. 1. It will be assumed that the ratio of volume flow to circulation is small so that in Region I, the primary flow region, the tangential velocity is a function of radius only. Region II consists of the boundary layers on both top and bottom end walls, in which axial velocity gradients and therefore axial viscous stresses become significant. Region III, bounded by an imaginary cylinder of radius equal to that of the exhaust hole, includes the flow in the vicinity of the axis of the tube, where both tangential and radial velocities vanish.

Appropriate solutions are employed in each of these regions and a consistent flow picture is obtained by application of suitable matching conditions. The solution of Lewellen,[7] which determines the circulation distribution in terms of the stream function, is used in Regions I and III. This solution becomes exact in the limit of large circulation and requires that the stream function be specified at the periphery of the applicable regions. The approximate boundary-layer solution of Rott[14] is used along the end walls, up to the edge of Region III, to provide a second relationship between the stream function and circulation in the primary flow, thereby establishing the interaction. The mathematical framework is completed with the specification of the stream function in Region III. Provision is included to allow the consideration of boundary-layer mass ejection due to the exhaust-hole discontinuity. Since little of a quantitative nature is known about this process at the present time, this phenomenon is treated parametrically. The fraction ζ of boundary-layer mass flow at the radius of the exhaust which is returned to the main flow before leaving the tube is introduced into the computational program and allowed to vary from zero to one. The complete set of equations is solved iteratively using a digital computer for a range of the governing parameters.

Before proceeding with the analysis, several comments are in order. First, the division of the flow into regions as indicated is not equivalent to the usual division of flows into a viscous boundary layer and an inviscid outer flow. In the present problem, the entire flow field is considered viscous; however, in the boundary layers the axial velocity gradients predominate, while in Regions I and III only the radial gradients are considered.

Second, the details of the flow in Region III are oversimplified as a result of insufficient knowledge. Recirculation of fluid originating downstream of the exhaust hole, which frequently occurs along the axis of the vortex tube, has been neglected. This can only be justified by the belief that such a phenomenon does not strongly influence the velocity distributions in Regions I and II.

Finally, a real, and possibly important, phenomenon is not considered at all in this paper, i.e., the boundary layer on the cylindrical containing walls and the details of the jet-mixing region if the vortex is driven by tangential fluid injection, as is commonly the case. These effects may influence the end-wall boundary-layer growth and will certainly make the determination of the peripheral circulation difficult in an actual experiment. For the present purposes, however, it is assumed that the outer cylinder is rotating and porous so that such questions may be avoided.

III. DERIVATION OF THE INTERACTION EQUATIONS

Consider a cylindrical coordinate system, r, θ, z, with associated velocity components u, v, w. The continuity and Navier-Stokes equations in these coordinates for an incompressible fluid with constant viscosity are:

$$\frac{\partial(ru)}{\partial r} + \frac{\partial(rw)}{\partial z} = 0 \tag{1}$$

$$u\frac{\partial u}{\partial r} + w\frac{\partial u}{\partial z} - \frac{v^2}{r} = -\frac{1}{\rho}\frac{\partial p}{\partial r} + \nu\left(\frac{\partial^2 u}{\partial r^2} + \frac{1}{r}\frac{\partial u}{\partial r} - \frac{u}{r^2} + \frac{\partial^2 u}{\partial z^2}\right) \tag{2}$$

$$u\frac{\partial v}{\partial r} + w\frac{\partial v}{\partial z} + \frac{uv}{r} = \nu\left(\frac{\partial^2 v}{\partial r^2} + \frac{1}{r}\frac{\partial v}{\partial r} - \frac{v}{r^2} + \frac{\partial^2 v}{\partial z^2}\right) \tag{3}$$

$$u\frac{\partial w}{\partial r} + w\frac{\partial w}{\partial z} = -\frac{1}{\rho}\frac{\partial p}{\partial z} + \nu\left(\frac{\partial^2 w}{\partial r^2} + \frac{1}{r}\frac{\partial w}{\partial r} + \frac{\partial^2 w}{\partial z^2}\right) \tag{4}$$

where the $\partial/\partial t$ and $\partial/\partial\theta$ terms have been eliminated by assuming the flow is steady and axisymmetric.

The axisymmetric stream function, ψ, is defined so that Eq. (1) is everywhere satisfied:

$$u = \frac{1}{r}\frac{\partial \psi}{\partial z} \quad ; \quad w = -\frac{1}{r}\frac{\partial \psi}{\partial r} \tag{5}$$

In addition, the dimensionless coordinates $\eta = (r/r_0)^2$ and $\xi = z/\ell$ and the quantities $\Omega = ur$ and $\Gamma = vr$ are introduced.

Lewellen[7] showed that $\partial\Gamma/\partial\xi$ was of order ϵ, where

$$\epsilon = \left(\frac{\psi_0}{\Gamma_0 r_0}\right)^2 \tag{6}$$

Therefore, in regions where the ratio of stream function to circulation is small, Γ may be considered independent of z, to order ϵ. Further, examination of Eq. (3) shows that when v is independent of z, the radial velocity, u, must also be independent of z (unless Γ = constant). In this case, Eq. (3) reduces to an ordinary, linear differential equation for Γ in terms of u and ν:

$$r^2 \frac{d}{dr}\left(\frac{1}{r}\frac{d\Gamma}{dr}\right) - \frac{ur}{\nu}\frac{d\Gamma}{dr} = 0 \tag{7}$$

The most general form of ψ, consistent with the condition that u be independent of z, is

$$\psi = Q_0 \ell [\xi f(\eta) + F(\eta)] \tag{8}$$

so that

$$u = \frac{Q_0}{r} f \qquad ; \qquad w = -\frac{2Q_0 \ell}{r_0^2}\left(\frac{z}{\ell} f' + F'\right)$$

Lewellen[7] has further shown that, since the equation which determines ψ is of order ϵ, to this order then the functions f and F remain to be determined by the boundary conditions.

In terms of f, η, and the radial Reynolds number $Re_r = Q_0/\nu$, Eq. (7) may be rewritten:

$$2\eta\Gamma'' - Re_r f\Gamma' = 0 \tag{9}$$

The functions ψ and Γ as defined by Eqs. (8) and (9) were shown by Lewellen[7] to be the zeroth order terms in a series expansion solution of Eqs. (1-4), in powers of ϵ.

Assuming the value of ϵ which characterizes the flow in Region III is also small, then Eq. (9) is valid for all r. Reference 15 contains further discussion of this assumption. Applying the boundary conditions

$$\Gamma = 0 \quad \text{at} \quad \eta = 0$$

$$\Gamma = \Gamma_0 \quad \text{at} \quad \eta = 1$$

Equation (9) may be integrated to give

$$\frac{\Gamma}{\Gamma_0} = c_1 \int_0^\eta \exp\left[\frac{Re_r}{2}\int_0^\eta \frac{f(\eta)}{\eta}\,d\eta\right] d\eta \tag{10}$$

where

$$c_1 = \frac{1}{\int_0^1 \exp\left[\frac{Re_r}{2}\int_0^\eta \frac{f(\eta)}{\eta}\,d\eta\right] d\eta}$$

Thus, with a given value of the radial Reynolds number and the radial distribution of f, the circulation distribution is uniquely determined.

It should be noted at this point that only f enters in the determination of Γ. That is, only that portion of the axial flow which is coupled to the radial flow through the continuity relationship plays a role.

The f-distribution, or equivalently the distribution of radial velocity through Regions I and III, will be determined by consideration of the end-wall boundary-layer flow. Since it is assumed that the boundary-layer mass flow grows from zero at r_0, any increase (or decrease) in the radial flow in the boundary layers must result in a corresponding decrease (or increase) in the radial flow through the primary vortex region. Thus, (in Region I),

$$f = 1 - \frac{2Q_{BL}}{Q_0'} \tag{11}$$

where

$$Q_{BL} = \int_0^{\delta} ru\, dz \tag{12}$$

There have been several analyses of the end-wall boundary-layer region.[11-14] For the present study, the results of the turbulent analysis of Rott[14] will be used. This is chosen because, at the tangential Reynolds numbers ordinarily encountered in vortex tubes, the boundary layers are most likely turbulent; and while Rott's analysis yields the simplest expression for the mass flow in the boundary layer, the results agree quite favorably with those of other, more complicated approaches. Assuming that the turbulent shear components are proportional to the squares of the respective velocity components and that the coefficient of friction so defined is constant, Rott, using a momentum-integral approximation, expressed the

volume flow in the boundary layer in terms of the Γ-distribution of the external flow as follows:

$$Q_{BL} = -ac\Gamma^{a-1} \int_0^x \Gamma^{2-a}\, dx \tag{13}$$

where $x = r_0 - r$, a = a velocity-profile shape parameter, and c = coefficient of friction. Following Rott, the values

$$a = 5 \quad ; \quad c = 0.027(Re_t)^{-1/5} \tag{14}$$

will be used for this study.

The specification of f in Region III is not quite so straightforward. As mentioned previously, the effect of the discontinuity at the edge of the exit hole (assumed here to be a sharp-edged orifice) and the question of recirculatory flow along the axis are not fully understood. In addition, there may be some question as to the validity of the boundary-layer analysis near the axis. All of these factors contribute to the difficulty of specifying f in detail in Region III. Fortunately, as far as the calculation of the circulation is concerned, only the integral of f appears in Eq. (10). Thus, Γ will be insensitive to the details of the axial velocity distribution (as long as v is independent of z). It will be assumed then that a certain fraction, ζ, of the boundary-layer volume flow at r_e (the radius of the exit hole), is ejected and returned to the primary flow to be redistributed into radial flow uniformly over the length of the tube. The quantity ζ will be considered parametrically in the computations, and its effect on the Γ- and f-distributions will be assessed. In addition, inside the radius of the exhaust, the simplest possible

assumption will be made, namely, that the radial velocity falls to zero at $r = 0$ linearly with r. Under these conditions

$$f = \left[1 - (1 - \zeta)\frac{2Q_{BL}(r_e)}{Q_0'}\right]\frac{r^2}{r_e^2} \tag{15}$$

when $r \leq r_e$.

Considering Eqs. (11), (13), (14) and (15), f may be written

$$f = 1 - A\left[\frac{\Gamma(\eta)}{\Gamma_0}\right]^4 \int_\eta^1 \left[\frac{\Gamma_0}{\Gamma(\eta)}\right]^3 \frac{d\eta}{2\sqrt{\eta}} \qquad ; \qquad 1 \geq \eta > \eta_e \tag{16}$$

$$f = \frac{\eta}{\eta_e}\left\{1 - (1 - \zeta)A\left[\frac{\Gamma(\eta_e)}{\Gamma_0}\right]^4 \int_{\eta_e}^1 \left[\frac{\Gamma_0}{\Gamma(\eta)}\right]^3 \frac{d\eta}{2\sqrt{\eta}}\right\} \qquad ; \qquad 0 \leq \eta \leq \eta_e$$

where

$$A = -\frac{0.27}{(Re_t)^{1/5}}\left(\frac{\Gamma_0 r_0}{Q_0'}\right) = \frac{2c\alpha}{\sqrt{\epsilon}} \tag{17}$$

Equations (10) and (17) determine f and Γ as functions of the radius and the parameters Re_r, A, r_e/r_0, and ζ. These equations have been solved iteratively using a digital computer for ranges of the governing parameters, and the results are presented and discussed in the next section.

IV. DISCUSSION OF RESULTS

The quantity A characterizes the boundary-layer interaction since it is a measure of the fraction of the total mass flow which passes through the boundary layer. If Γ were constant and equal to Γ_0 for all r, then it can be seen from Eqs. (13), (14), and (16) that A would be equal to the fraction of the total mass flow in the boundary layers at r = 0. Also, from Eq. (17) it is seen that $A \sim 1/\epsilon^{1/2}$, so that small values of ϵ ordinarily correspond to large values of the boundary-layer interaction parameter. Thus, it is precisely in the regime where Γ is independent of z that the end-wall boundary-layers will play a significant role in the determination of the radial Γ-distribution.

An interesting exception occurs in the limit of A going to zero as a result of frictionless, or suitably rotating, end walls (i.e., not because ϵ becomes large). In this case, the present problem becomes identical with that considered by Einstein and Li.[5] The stream function is given simply by

$$f = 1 \quad ; \quad \eta > \eta_e$$

$$f = \eta/\eta_e \quad ; \quad \eta < \eta_e \tag{18}$$

and Eq. (10) yields the circulation distribution

$$\frac{\Gamma}{\Gamma_0} = \frac{2}{Re_r}\frac{\eta_e}{K}\left[\exp\left(\frac{Re_r\eta}{2\eta_e}\right) - 1\right] \quad ; \quad \eta \le \eta_e$$

$$\frac{\Gamma}{\Gamma_0} = \frac{\eta_e \exp(Re_r/2)}{([Re_r/2] + 1)}\left[\left(\frac{\eta}{\eta_e}\right)^{(Re_r/2)+1} - 1\right] \tag{19}$$

$$+ \frac{2\eta_e}{Re_r K}\left[\exp\left(\frac{Re_r}{2}\right) - 1\right] \quad ; \quad \eta \ge \eta_e$$

where

$$K = \frac{\eta_e \exp(Re_r/2)}{(Re_r/2) + 1}\left[\eta_e^{-([Re_r/2]+1)} - 1\right] + \frac{2\eta_e}{Re_r}\left[\exp\left(\frac{Re_r}{2}\right) - 1\right]$$

This solution is shown in Fig. 5 for three values of the radial Reynolds number and $r_e/r_0 = 1/6$.

Another interesting limiting case, which may be solved analytically, occurs when $Re_r \to -\infty$. This case has been solved in Appendix A. In this limit, the circulation distribution remains constant for $A < 0(1)$. For $A > 0(1)$, the circulation remains constant with decreasing radius from r_0 until all of the flow reaches the end-wall boundary layers. Between this radius and the edge of the exhaust hole the total radial flow remains in the boundary layers and the circulation distribution is that required to drive this boundary-layer flow.

Results of the digital computer solutions for Γ- and f-distributions corresponding to various combinations of the governing parameters are shown in Figs. 6 through 10. All of these results were obtained for a constant value of $r_e/r_0 = 1/6$. The successive figures correspond to increasing values of A. Values of radial Reynolds number have been chosen so that results representative of the distributions obtainable are presented. In most of these figures, curves are plotted only for $\zeta = 0$ and $\zeta = 1$, since results for intermediate values may be easily inferred from those presented. In Fig. 7, the curve for $\zeta = 0.5$ is also presented, indicating a rather uniform variation of the distributions with ζ between the extremes of zero and one. Results of the analytical solution of Appendix A for $Re_r = -\infty$ are included in Figs. 8-10.

The curves illustrate that when $A \leq 1$, the effect of the boundary-layer interaction is relatively small. The same is true when $|Re_r|$ is small regardless of the value of A. In both of these areas, of course, the influence of ζ is also small. For slightly larger values of A, the boundary-layer

interaction begins to exert a considerable influence, especially at the higher values of $|Re_r|$. The effect of ζ also becomes more pronounced here. A value of $\zeta = 1$ causes the circulation distribution to stay closer to a constant and results in increases of Γ_e/Γ_0 of up to 20 percent. Its influence on the mass-flow distribution is more profound (as seen in Figs. 7 and 8), resulting in negative values of f, which implies that the boundary-layer mass flow is locally greater than the total through-flow so that radial outflow must exist in the primary-flow region. It is interesting to note that in spite of this excess mass flow in the boundary layers, the Γ-distribution remains essentially constant.

At still larger values of the interaction parameter, the Γ-distribution decreases faster (see Figs. 9 and 10), and the theoretical results for infinite Reynolds number are approximated closely by those for more moderate Reynolds numbers.

In order to characterize the effect of the interaction in a simple way, the value of Γ_e/Γ_0 is plotted in Fig. 11 as functions of A and Re_r for $r_e/r_0 = 1/6$. This curve also illustrates the influence of ζ. It is seen that for $\zeta = 0$, values of Γ_e/Γ_0 begin to depart from one when $A > 1.2$, even for infinite Reynolds number. For $\zeta = 1$, this departure is delayed until $A > 2.2$. The same results are cross-plotted in different ways in Figs. 12 and 13. Figure 12 shows Γ_e/Γ_0 vs Re_r for constant A, including the $A = 0$ results. At $A = 1$ and $\zeta = 1$, it is seen that Γ_e/Γ_0 values of 0.98 are achieved for $|Re_r| > 13$, while this does not occur for $\zeta = 0$ until $|Re_r| > 40$. This is illustrated more clearly in Fig. 13, which shows curves of constant Γ_e/Γ_0 as functions A and Re_r.

The mass flow distributions are characterized by the minimum value of f (designated f_m) and the amount of fluid which is returned by the boundary layers to the primary flow ($f_e - f_m$). These distributions are plotted in Figs. 14 and 15. Negative values of f_m indicate reverse flow regions in the primary flow.

In order to assess the influence of r_e on the Γ- and f-distributions, solutions were obtained for specific combinations of A and Re_r for $r_e/r_0 = 1/4$ and $1/10$, in addition to the results already presented for $r_e/r_0 = 1/6$. Typical profiles are shown in Fig. 16, illustrating that Γ_e/Γ_0 and f_m tend to increase with increasing r_e/r_0 although, at a given radius, increasing r_e/r_0 tends to decrease Γ. Results for Γ_e/Γ_0 and f_m are shown as functions of r_e/r_0 in Figs. 17 and 18, demonstrating the relative influence of exhaust radius in various regimes.

In Appendix B, the effects of compressibility are considered by treating the isothermal case. It is shown that the present results are accurate for most practical applications.

V. COMPARISON WITH EXPERIMENT AND COMMENTS REGARDING TURBULENCE

It has been traditional to compare experimental results and theory by matching the measured circulation distributions (deduced from static pressure measurements) with the analytical predictions. In all cases, it has been found that circulation profiles could be matched only when the measured laminar radial Reynolds number was much higher than its theoretical counterpart. As mentioned in the introduction, previous investigations of vortex flow in tubes were based on one-dimensional flow models (equivalent to setting $A = 0$ in the present theory) and tended to ascribe discrepancies between measured and theoretically computed circulation profiles to the presence of turbulence in the flow field. It was assumed that the turbulence produced a large "eddy viscosity" which in turn resulted in a reduced radial Reynolds number. The ratio of the theoretically deduced "effective" radial Reynolds number to the actual radial Reynolds number based on a laminar viscosity was used as a measure of the turbulence level in the tube. Thus, Keyes,[8] for example, was able to arrive at a correlation between apparent turbulence level and the tangential peripheral Reynolds number of the flow.

Subsequently, Kendall[17] and others pointed out the significance of the end-wall boundary-layer interaction and suggested that the reduction in Γ-distribution, which had been attributed to turbulence, may indeed be explainable largely or wholly by the three-dimensional boundary-layer interaction. It was argued that diversion of flow into the boundary layers reduced the radial Reynolds number in the primary flow, thus accounting for the reduced values of Γ/Γ_0.

As the present study shows, however, when Γ/Γ_0 begins to depart from one, the boundary-layer growth slows down and finally reverses, resulting in fluid being returned to the primary flow. Since only a fraction of the fluid's angular momentum is lost in the boundary layer (on the average),

mass ejection from the boundary layer tends to support the angular momentum distribution, retarding its further decline. Finite values of ζ contribute further to this trend, resulting, as has been seen, in the requirement that A be greater than 1.2 for $\zeta = 0$ (or 2.2 if $\zeta = 1$) before any significant degradation of the Γ-profile occurs due to the boundary-layer interaction.

In order to determine whether three-dimensionality can indeed explain all or part of the experimentally observed velocity distributions, some new experiments were conducted, using two different vortex chambers. Somewhat modified versions of the apparatus described by Rosenzweig[19] and Grabowsky and Rosenzweig[20] were used. These tests will not be described in detail; only the results will be presented here. The data were reduced using the present theory to infer a value of "effective" radial Reynolds number, after Γ_e and the value of A had been determined from measured quantities. (Note: Because of the difficulties associated with the experimental determination of Γ_0, the ratio $\Gamma_e/\Gamma_{1/2}$ was used to compare with the theory.) Results of these tests are shown in Fig. 19 as a ratio of actual to "effective" radial Reynolds numbers vs tangential Reynolds number based on tube diameter. A spread is indicated for each test point, the upper bound corresponding to $\zeta = 1$ and the lower to $\zeta = 0$. For some of the tests, an independent calculation of the turbulent shear stress is made possible by means of a torque-balance measurement. Such results can also be reduced to a ratio of Reynolds numbers and these points are indicated in Fig. 19 as well. Also included are several hot-wire measurements of Kendall.[17] Keyes' least-squares curve[8] is shown for comparison, as are some of his actual test points.

Values of A in these experiments ranged from 0.6 to 1.5 and radial Reynolds numbers varied from 12 to several thousand. Calculations indicate that values of A of order one were also representative of Keyes' experiments. The conclusion is, therefore, that early estimates of turbulence levels in jet-driven vortices, although based on one-dimensional flow models,

were not greatly in error. Furthermore, the close agreement in Reynolds number ratio between the results based on the theory as presented herein and independent measurements of turbulent shear lend credence to the present theory.

VI. CONCLUSIONS

The equations governing the interaction between the primary flow and end-wall boundary layers in a vortex tube have been presented and solved iteratively on a digital computer. The controlling parameters include a boundary-layer interaction parameter, A, representing a measure of the mass fraction diverted to the boundary layers; the radial Reynolds number; and a parameter, ζ, representing the boundary-layer mass ejection occurring as a result of the geometrical discontinuity existing at the exhaust-hole radius. Circulation and mass-flow distributions are presented, illustrating the variety of results obtainable in the different flow regimes. Over-all results are characterized by the values of Γ_e/Γ_0, the circulation ratio at the exhaust radius, and f_m, the minimum mass flow in the primary flow region.

The results show that if $A < 1$, the effect of the boundary layer interaction on the circulation distribution is small. The same is true if $|Re_r|$ is of order one, regardless of A. As A increases, the effect is more pronounced, the interaction producing a reduced Γ_e/Γ_0 and f_m. A variation of ζ from zero to one produces a maximum increase of approximately 20 percent in Γ_e/Γ_0, but can have a profound effect on f_m, causing negative values (i.e., reverse flow) to occur in some instances. It has been shown that in some cases it is possible to have an excess of flow in the boundary layer (i.e., $f_m < 0$) while Γ/Γ_0 remains close to unity.

The influence of exhaust radius variation has been investigated and, in addition, analytical solutions for the limiting cases of $A = 0$ and $Re_r \to -\infty$ have been presented.

The theoretical results have been compared with experiments by matching experimental and theoretical circulation profiles and thereby determining a ratio of "actual" (laminar) to "effective" radial Reynolds number. By comparison with previous results it has been concluded that

turbulence levels in jet-driven vortex flows are high and that estimates based on one-dimensional assumptions were not greatly in error.

APPENDIX A

ANALYTIC SOLUTION FOR INFINITE REYNOLDS NUMBER

An analytic solution to Eqs. (10) and (16) is possible in the limit of $Re_r \to -\infty$. From Eq. (9) it is seen that in order to have a finite value of f in this limit, either an infinity or a zero in Γ' is required. Conversely, any Γ-distribution is possible when f = 0, since the product $Re_r f$ is then indeterminate. Therefore, it is evident that in this limit Γ will remain constant at large radii until all of the flow reaches the end-wall boundary layers, i.e., until f = 0. Proceeding inward from this point, all the flow will remain in the boundary layers, and the circulation will distribute itself in just such a way as to keep f = 0. This distribution may be found by writing Eq. (13) in differential form:

$$\frac{d}{dr} Q_{BL} \Gamma - a Q_{BL} \frac{d\Gamma}{dr} = ac\Gamma^2 \tag{A-1}$$

For Q_{BL} = constant, this reduces to

$$\frac{1}{\Gamma^2} \frac{d\Gamma}{dr} = \frac{ac}{Q_{BL}(1 - a)} \tag{A-2}$$

Equation (A-2) integrates to

$$\frac{\Gamma_0}{\Gamma} = \frac{A}{(1 - a)(1 - f)} \frac{r}{r_0} + c_2 \tag{A-3}$$

in terms of previously defined dimensionless parameters. The constant c_2 is evaluated by the condition that $\Gamma/\Gamma_0 = 1$ at $r = \hat{r}$, the radius at which f first reaches zero. For $r > \hat{r}$, from Eqs. (11) and (13),

$$f = 1 - A[1 - (r/r_0)] \tag{A-4}$$

Therefore,

$$\hat{r}/r_0 = 1 - 1/A \tag{A-5}$$

From Eq. (A-5) and the condition that $\Gamma/\Gamma_0 = 1$, $f = 0$ at $r = \hat{r}$, Eq. (A-3) reduces to

$$\frac{\Gamma}{\Gamma_0} = \frac{\alpha - 1}{\alpha - 2 + A[1 - (r/r_0)]} \quad ; \quad r < \hat{r} \tag{A-6}$$

For $\zeta = 0$, the solution for the Γ-distribution in the limit of $Re_r \to -\infty$ is $\Gamma = \Gamma_0$ for $r > \hat{r}$ and is given by Eq. (A-6) for $r_e < r < \hat{r}$. Inside the exhaust radius it is undetermined.

The solution for $\zeta \neq 0$ is slightly different. At the radius of the exhaust, flow is forced out of the boundary layer so that $f > 0$ when $r < r_e$. Thus Γ' must be zero here from Eq. (9). Furthermore, differentiation of Eq. (10) indicates that Γ' must remain zero for $r > r_e$ until

$$\int_0^{\eta} \frac{f}{\eta}\, d\eta \leq 0 \tag{A-7}$$

This in turn requires f to be negative in some region outside the radius of the exhaust. Thus, for $\zeta \neq 0$, Eq. (A-6) applies only to $r > r^*$, with r^* defined so that

$$\int_0^{\eta^*} \frac{f}{\eta}\, d\eta = 0 \qquad \text{(A-8)}$$

To complete Eq. (A-8), f is given by

$$f = \frac{\eta}{\eta_e}\left[1 + (1 - \zeta)(f_e - 1)\right] \quad ; \quad \eta < \eta_e$$

$$f = A\frac{\Gamma_e}{\Gamma_0}(\sqrt{\eta} - \sqrt{\eta^*}) \quad ; \quad \eta_e < \eta < \eta^* \qquad \text{(A-9)}$$

Equations (A-8) and (A-9) yield an algebraic equation relating Γ_e and η^*:

$$1 - (1 - \zeta)\left[1 - A\frac{\Gamma_e}{\Gamma_0}(\sqrt{\eta} - \sqrt{\eta^*})\right] = A\frac{\Gamma_e}{\Gamma_0}\left[\sqrt{\eta^*}\ln\frac{\eta^*}{\eta_e} - 2(\sqrt{\eta^*} - \sqrt{\eta_e})\right] \qquad \text{(A-10)}$$

A second equation relating Γ_e and η^* is obtained from Eq. (A-6) which is valid at η^*:

$$\frac{\Gamma_e}{\Gamma_0} = \frac{a - 1}{a - 2 + A(1 - \sqrt{\eta^*})} \qquad \text{(A-11)}$$

Equations (A-10) and (A-11) must be solved simultaneously to obtain Γ_e and η^*. A representative result is shown in Fig. 9.

APPENDIX B

COMPRESSIBILITY EFFECT

In the applications and experiments referred to in the introduction, velocities of the order of the speed of sound may be expected to occur within the vortex. Under such conditions the assumption of incompressible flow might appear to be a source of considerable error. The purpose of this appendix is to prove that incompressible flow is still a valid assumption for this problem.

A complete solution of the compressible problem necessarily involves a solution of the energy equation and a means of accounting for the energy sources and sinks within the flow and on the boundaries of the flow. Such conditions will vary widely for the applications considered. To avoid this complexity, for the present purposes the flow will be assumed to be isothermal (i.e., Prandtl number equal to zero). The isothermal assumption provides the most stringent test of the effects of compressibility (as long as there are no heat sources or sinks present) since for this case the density change due to pressure variation will be a maximum. For isothermal flow, it is also consistent to keep viscosity, μ, a constant. Under these conditions the only one of Eqs. (1) through (4) to change is Eq. (1), which should now be written as

$$\frac{\partial}{\partial r}(\rho u r) + \frac{\partial}{\partial z}(\rho w r) = 0 \qquad \text{(B-1)}$$

This calls for redefining the stream function, ψ, as

$$\rho u = \frac{\rho_0}{r}\frac{\partial \psi}{\partial z} \quad ; \quad \rho w = -\frac{\rho_0}{r}\frac{\partial \psi}{\partial r} \qquad \text{(B-2)}$$

With this extended definition of ψ, Eqs. (8) and (10) are unchanged as the solution of the flow in Regions I and III.

In Region II, the assumption of isothermal flow implies that the density gradient across the boundary layer can be ignored, while the radial variation of density must be retained. In Rott's notation, the momentum integral equation in the tangential direction with $\rho = \rho(r)$ is

$$\frac{d}{dx}\rho \int_0^\infty ur^2(V - v)\, dz - \rho \frac{d}{dx}(rV) \int_0^\infty ur\, dz = r^2 \tau_\phi \qquad \text{(B-3)}$$

The solution of Eq. (B-3), which replaces Eq. (13), is

$$Q_{BL} = -\frac{a}{\rho} c \Gamma^{a-1} \int_0^x \rho \Gamma^{2-a}\, dx \qquad \text{(B-4)}$$

Since it is now mass flow which is conserved rather than volume flow, Eq. (11) must also be altered to give:

$$f = 1 - \frac{2\rho Q_{BL}}{\rho_0 Q_0 \Gamma} \qquad \text{(B-5)}$$

Keeping the assumption of linear decay of the radial mass flow within the exhaust radius, and using Eqs. (B-4) and (B-5), Eq. (16) now becomes

$$f = 1 - A\left(\frac{\Gamma(\eta)}{\Gamma_0}\right)^4 \int_\eta^1 \frac{\rho(\eta)}{\rho_0}\left(\frac{\Gamma_0}{\Gamma(\eta)}\right)^3 \frac{d\eta}{2\sqrt{\eta}} \quad ; \quad 1 \geq \eta > \eta_e$$

$$f = \frac{\eta}{\eta_e}\left[1 - (1-\zeta)A\left(\frac{\Gamma(\eta_e)}{\Gamma_0}\right)^4 \int_{\eta_e}^1 \frac{\rho(\eta)}{\rho_0}\left(\frac{\Gamma_0}{\Gamma(\eta)}\right)^3 \frac{d\eta}{2\sqrt{\eta}}\right] \quad ; \quad 0 \leq \eta \leq \eta_e \qquad \text{(B-6)}$$

Equations (B-6) and (10) are the extended equations replacing Eqs. (16) and (10) as the equations to be solved iteratively on the computer. The system is now completed by using Eq. (2) to determine the pressure and consequently the density distribution. Neglecting order ϵ, Eq. (2) gives

$$\frac{1}{\rho}\frac{\partial p}{\partial r} = \frac{v^2}{r} \qquad \text{(B-7)}$$

From the equation of state

$$\rho = [p/(RT)] \qquad \text{(B-8)}$$

Equation (B-7) can be written as

$$\frac{1}{p}\frac{\partial p}{\partial r} = \frac{1}{RT}\frac{\Gamma^2}{r^3} \qquad \text{(B-9)}$$

which for isothermal flow integrates to

$$\frac{p}{p_0} = \exp\left\{-\frac{\gamma M_0^2}{2}\int_\eta^1 \left[\frac{\Gamma(\eta)}{\Gamma_0}\right]^2 \frac{d\eta}{\eta^2}\right\} \qquad \text{(B-10)}$$

with γ the ratio of specific heats and M_0 the tangential Mach number at r_0. It follows directly from Eqs. (B-8) and (B-10) that

$$\frac{\rho}{\rho_0} = \exp\left\{-\frac{\gamma M_0^2}{2}\int_{\eta}^{1}\left[\frac{\Gamma(\eta)}{\Gamma_0}\right]^2\frac{d\eta}{\eta^2}\right\} \qquad \text{(B-11)}$$

The addition of Eq. (B-11) to determine ρ/ρ_0 in Eq. (B-6) does not greatly complicate the iteration scheme, which is still carried through in the same manner. It is only necessary to add a loop determining ρ/ρ_0 from the Γ obtained in the previous step. There is, however, a new parameter, γM_0^2, affecting the solutions.

Figure B-1 compares the Γ- and f-distributions with and without the compressibility effect for several sets of values of the parameters, corresponding roughly to the limiting Mach numbers obtained in the experiments discussed in the paper. Although Mach numbers above 2 are obtained, the effect of compressibility on the distributions of Γ and f is small. It is, of course, possible to increase the theoretical values of M_0 to the point where the density variation would cause a large change in the Γ-distribution, but Mach numbers of such a magnitude have never been obtained experimentally. Also, an increase of A, with M_0 constant, will produce a larger compressibility effect since the primary effect of compressibility is manifested through the boundary layer interaction.

ACKNOWLEDGMENT

The authors wish to acknowledge the contribution of Jack Macki and Irene Wong of the Aerospace Computation and Data Processing Center for the programming and computation of data used in this report.

REFERENCES

1. Lewellen, W. S., and W. R. Grabowsky, "Nuclear Space Power Systems Using Magnetohydrodynamic Vortices," ARS J. (May 1962).

2. Kerrebrock, J. L., and R. V. Meghreblian, "Vortex Containment for the Gaseous Fission Rocket," J. Aerospace Sci. (September 1961).

3. Donaldson, C. duP., and R. D. Sullivan, "Behavior of Solutions of the Navier-Stokes Equations for a Complete Class of Viscous Vortices," Proc. Heat Transfer and Fluid Mech. Inst., Stanford Univ. Press (1960).

4. Deissler, R. G., and M. Perlmutter, "An Analysis of the Energy Separation in Laminar and Turbulent Compressible Vortex Flows," Proc. Heat Transfer and Fluid Mech. Inst., Stanford Univ. Press (1958).

5. Einstein, H. A., and H. Li, "Steady Vortex Flow in a Real Fluid," Proc. Heat Transfer and Fluid Mech. Inst., Stanford Univ. Press (1951).

6. Anderson, O., "Theoretical Solutions for the Secondary Flow on the End Wall of a Vortex Tube," UAC Research Laboratories Report R-2494-1, United Aircraft Corporation, East Hartford, Connecticut (November 1961).

7. Lewellen, W. S., "A Solution for Three-Dimensional Vortex Flows with Strong Circulation," J. Fluid Mech. 14 (3), (1962).

8. Keyes, J. J., Jr., "An Experimental Study of Flow and Separation in Vortex Tubes with Application to Gaseous Fission Heating," ARS J. (September 1961).

9. Ragsdale, R. G., "NASA Research on the Hydrodynamics of the Gaseous Vortex Reactor," NASA TN-D-288 (June 1960).

10. Taylor, G. I., "The Boundary Layer in the Converging Nozzle of a Swirl Atomizer," Quart. J. Mech. Appl. Math. 3 (1950).

11. Mack, L. M., "Laminar Boundary Layer on a Disk of Finite Radius in a Rotating Flow, Part I," Jet Propulsion Laboratory TR-32-224 (May 20, 1962).

REFERENCES (Continued)

12. King, W. S., "Momentum Integral Solutions for the Laminar Boundary Layer on a Finite Disk in a Rotating Flow," Aerospace Corporation ATN-63(9227)-3 (June 18, 1963).

13. Weber, H. E., "Boundary Layer Inside a Conical Surface due to Swirl," J. Appl. Mech. (Series E of ASME Transactions) 23 (1956).

14. Rott, N., "Turbulent Boundary Layer Development on the End Walls of a Vortex Chamber," Aerospace Corporation ATN-62(9202)-1 (July 30, 1962).

15. Lewellen, W. S., "Three-Dimensional Viscous Vortices in Incompressible Flow," Ph. D. Thesis, University of California at Los Angeles, 1964.

16. Rosenzweig, M. L., D. H. Ross, and W. S. Lewellen, "On Secondary Flows in Jet-Driven Vortex Tubes," J. Aerospace Sci. 29 (September 1962).

17. Kendall, J. M., Jr., "Experimental Study of a Compressible Viscous Vortex," Jet Propulsion Laboratory TR-32-290 (June 5, 1962).

18. Ross, D. H., "An Experimental Study of Secondary Flow in Jet-Driven Vortex Chambers," Aerospace Corporation ATN-64(9227)-1 (1964).

19. Rosenzweig, M. L., "Summary of Research in the Field of Advanced Nuclear Propulsion," Semiannual Technical Report, Aerospace Corporation TDR-930(2210-14)TR-1 (10 March 1962).

20. Grabowsky, W. R., and M. L. Rosenzweig, "Advanced Propulsion," Semiannual Technical Note, Aerospace Corporation ATN-63(9227)-2 (30 April 1963).

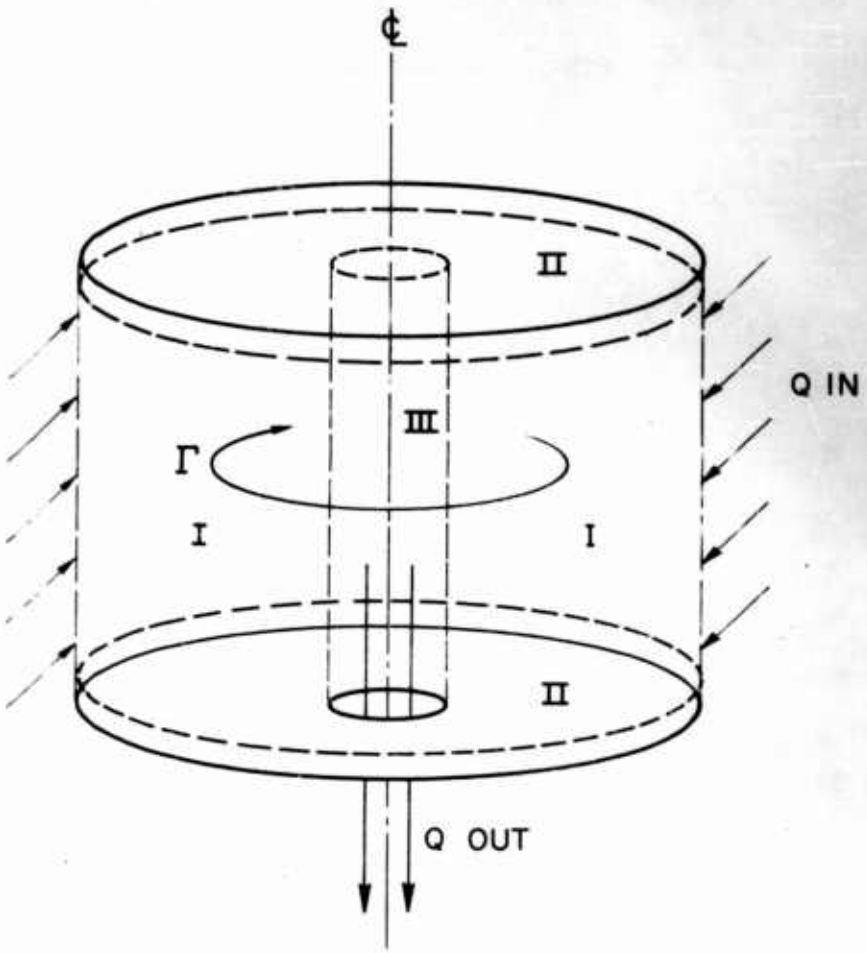

Fig. 1. Vortex Tube Geometry Showing Division of Flow into the Three Regions Described in the Paper

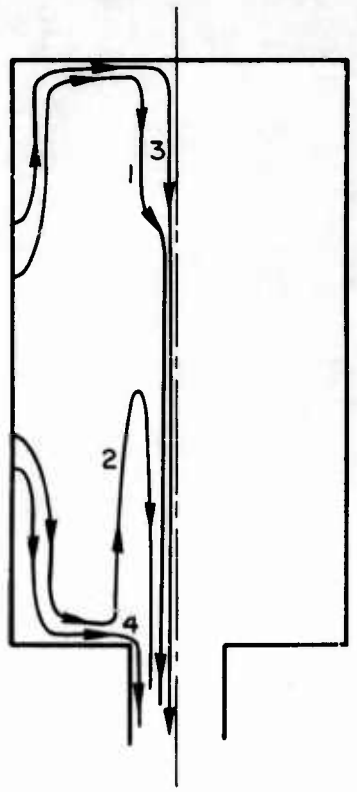

Fig. 2. Possible Streamline Patterns in the Vortex Tube

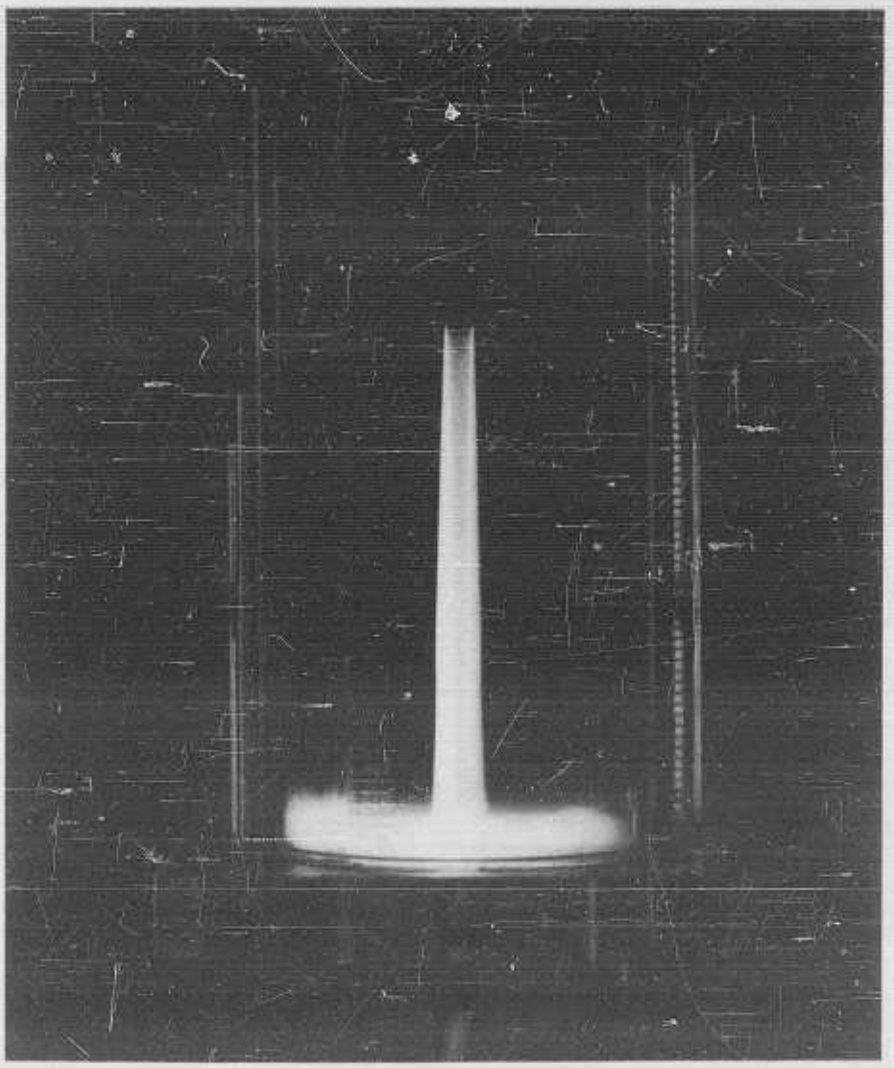

Fig. 3. Vortex Flow Visualization Picture with Dye Injected into the Boundary Layer, Showing Mass Ejection in Vicinity of Exhaust Radius

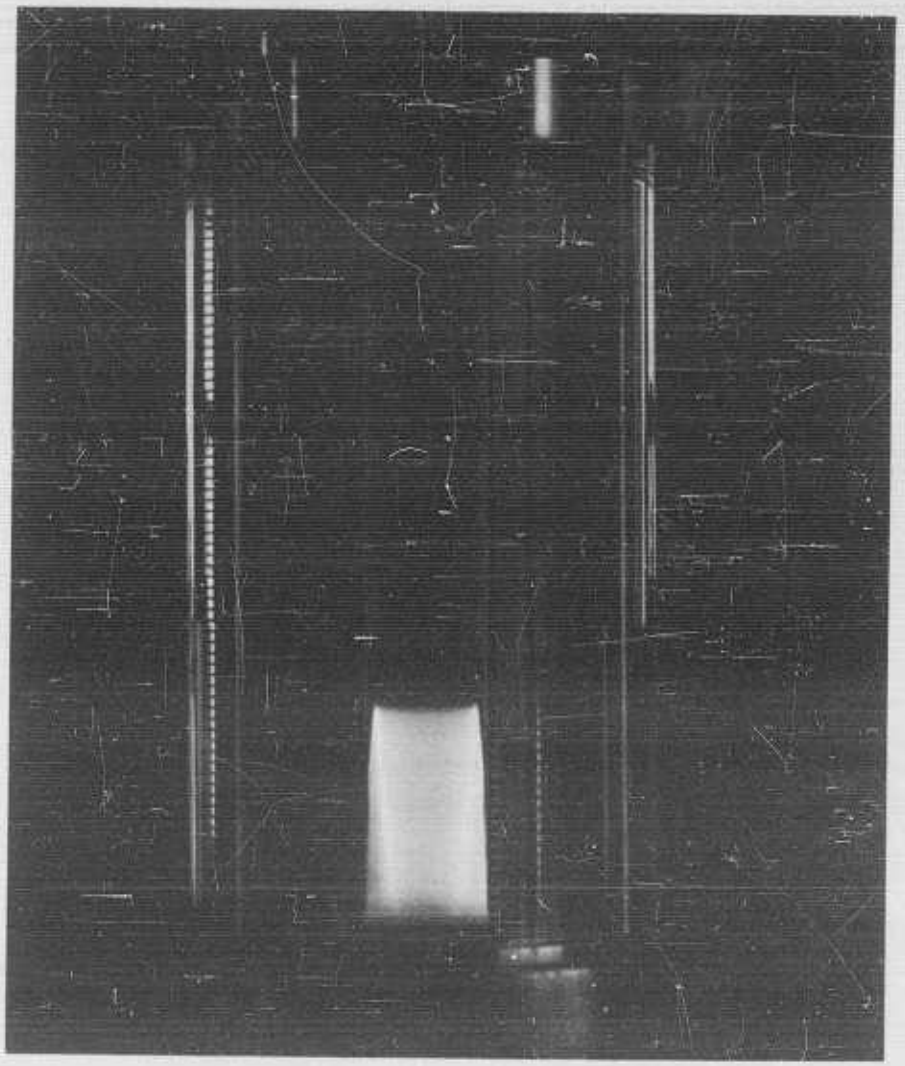

Fig. 4. Vortex Flow Visualization Picture with Dye Injected into the Boundary Layer, with a Stepped-Down End Wall Showing Mass Ejection in Neighborhood of Step

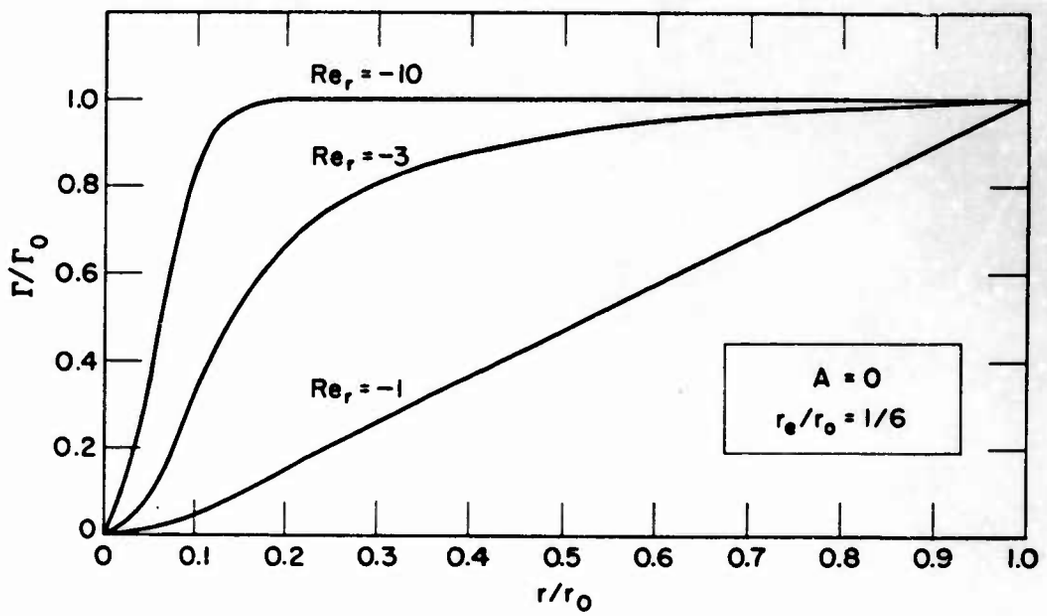

Fig. 5. Circulation Distributions as a Function of Radius for A = 0

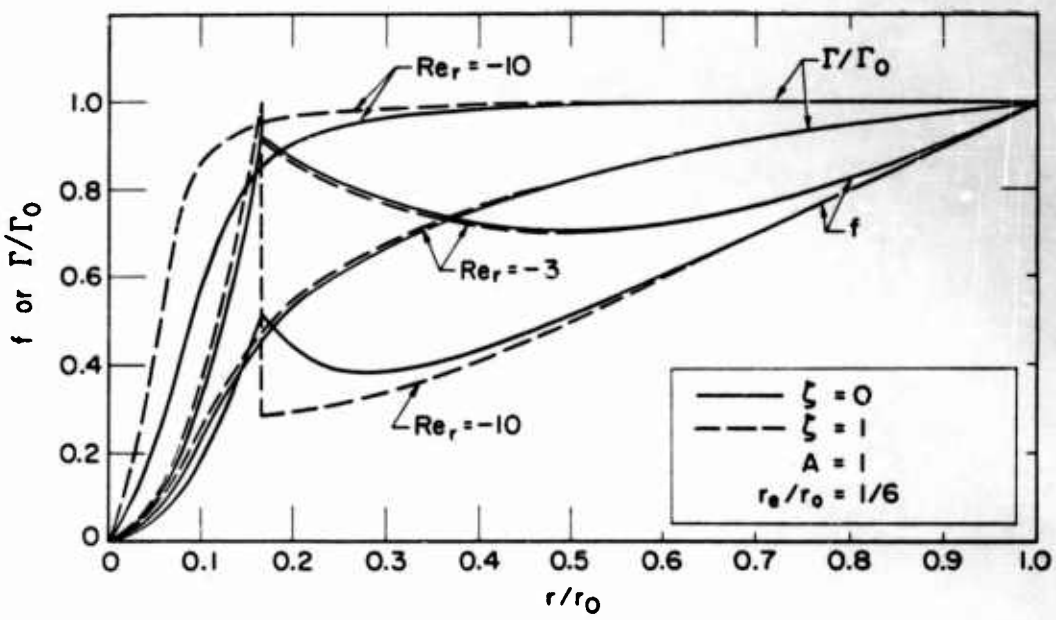

Fig. 6. Circulation and Stream Function Distributions as a Function of Radius for A = 1

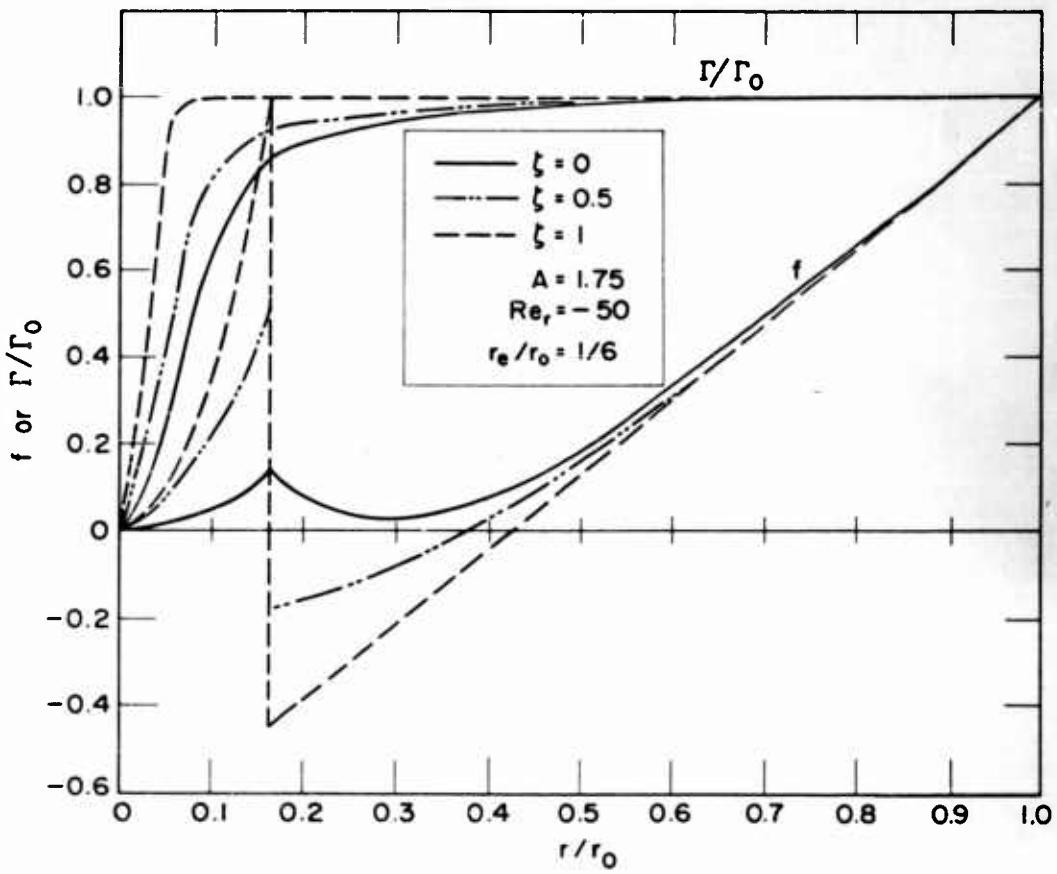

Fig. 7. Circulation and Stream Function Distributions as a Function of Radius for A = 1.75 and Re_r = -50

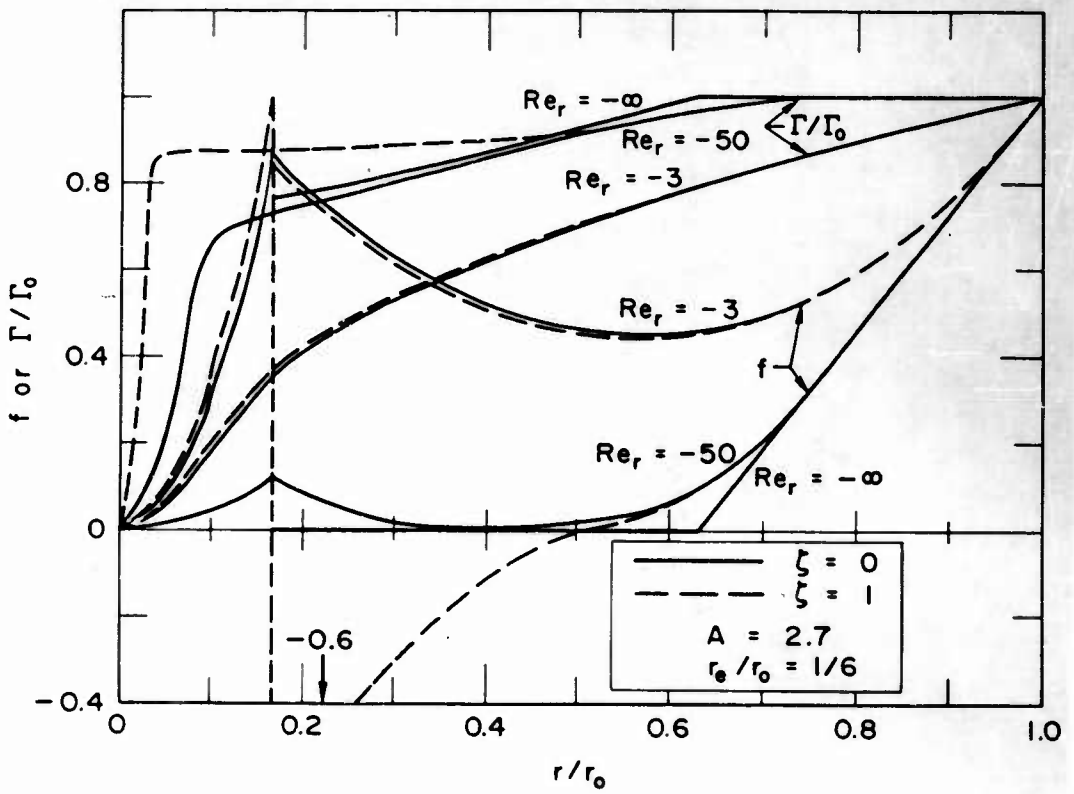

Fig. 8. Circulation and Stream Function Distributions as a Function of Radius for A = 2.7

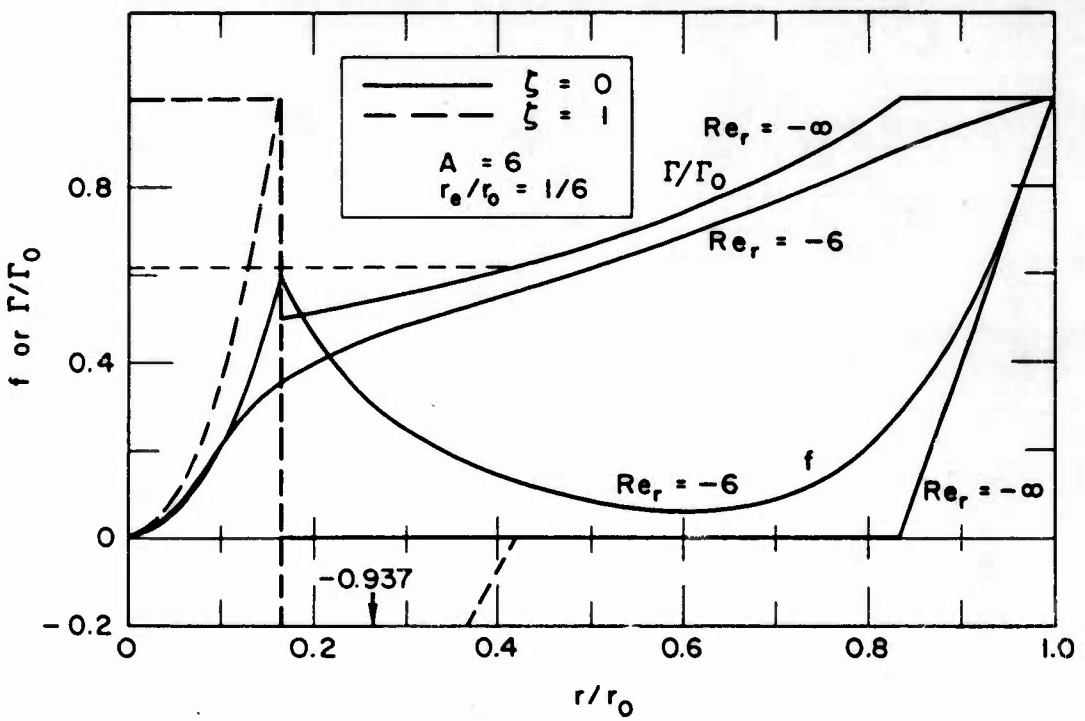

Fig. 9. Circulation and Stream Function Distribution as a Function of Radius for A = 6

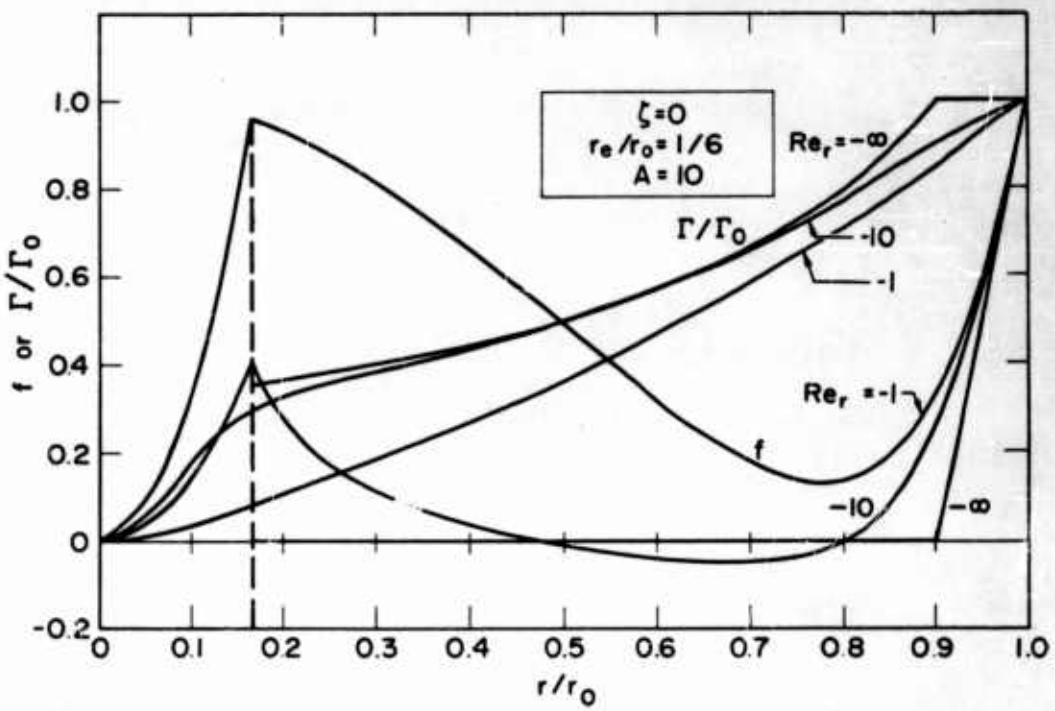

Fig. 10. Circulation and Stream Function Distribution as a Function of Radius for A = 10

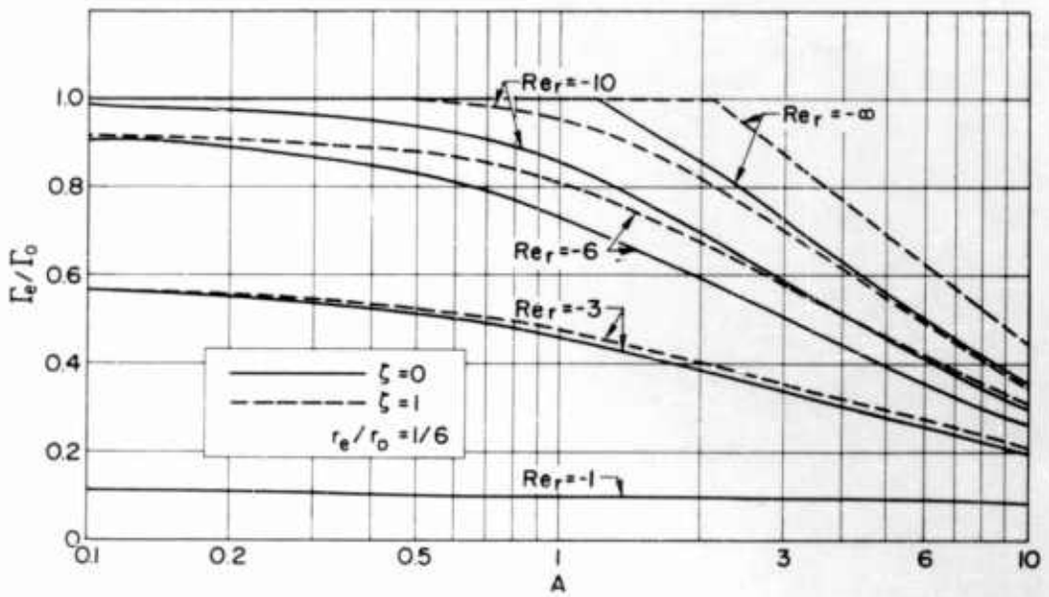

Fig. 11. Circulation at the Edge of the Exhaust Hole as a Function of A for Constant Re_r

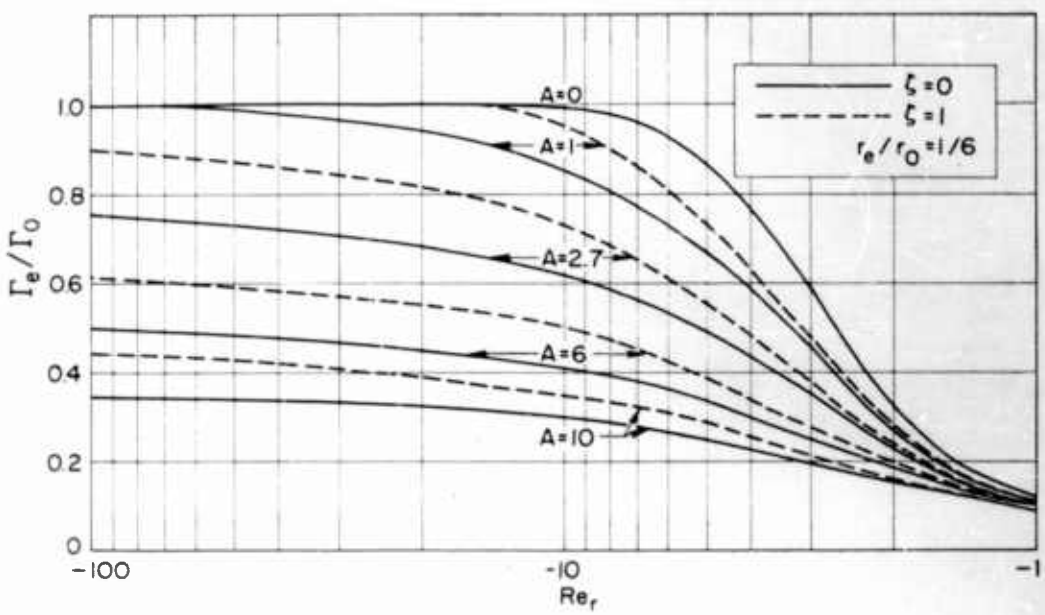

Fig. 12. Circulation at the Edge of the Exhaust Hole as a Function of Re_r for Constant A

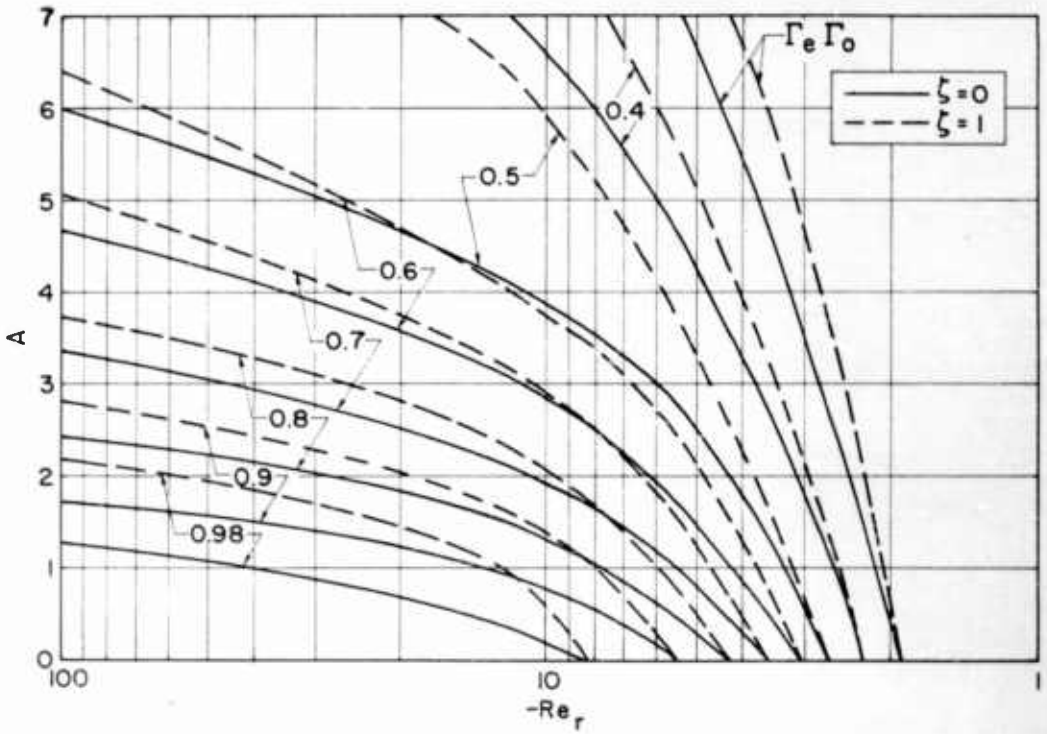

Fig. 13. A as a Function of Re_r for Constant Circulation at the Edge of the Exhaust Hole

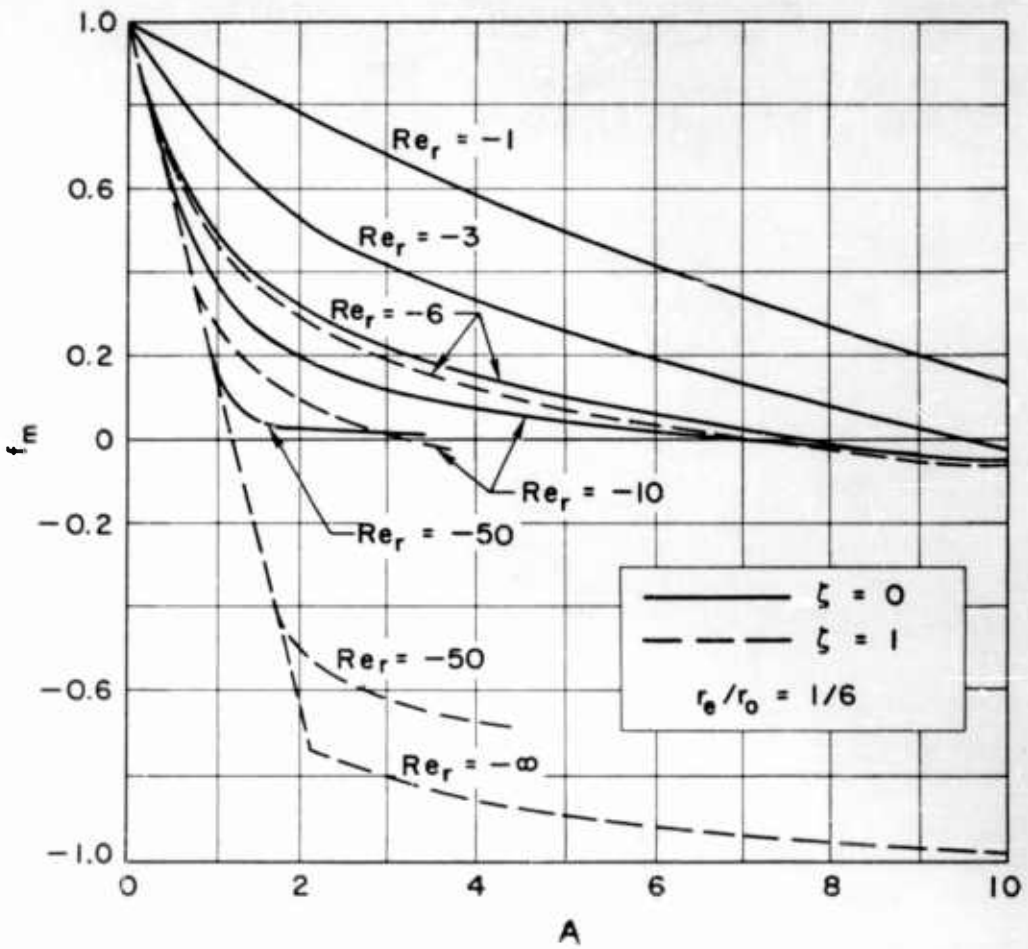

Fig. 14. Minimum Mass Flow in the Primary Flow Region as a Function of A for Constant Re_r

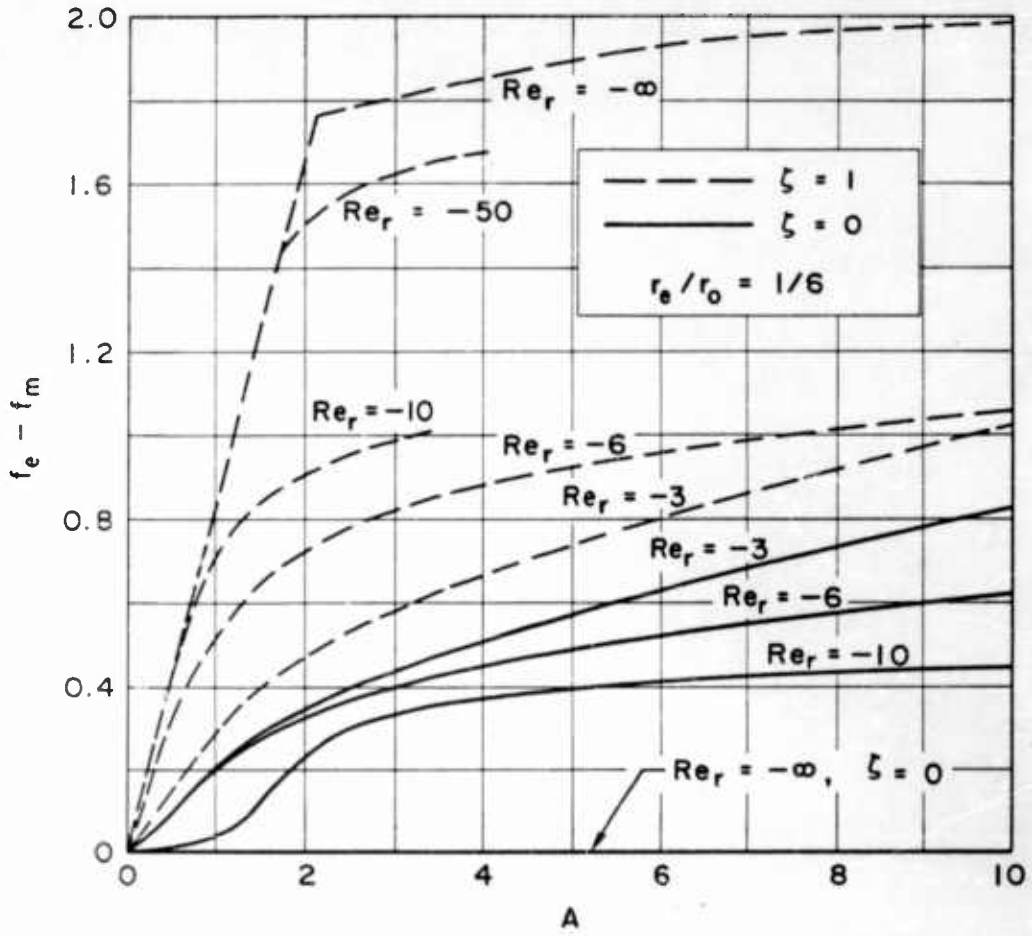

Fig. 15. Amount of Fluid Returned by the Boundary Layers to the Primary Flow as a Function of A for Constant Re_r

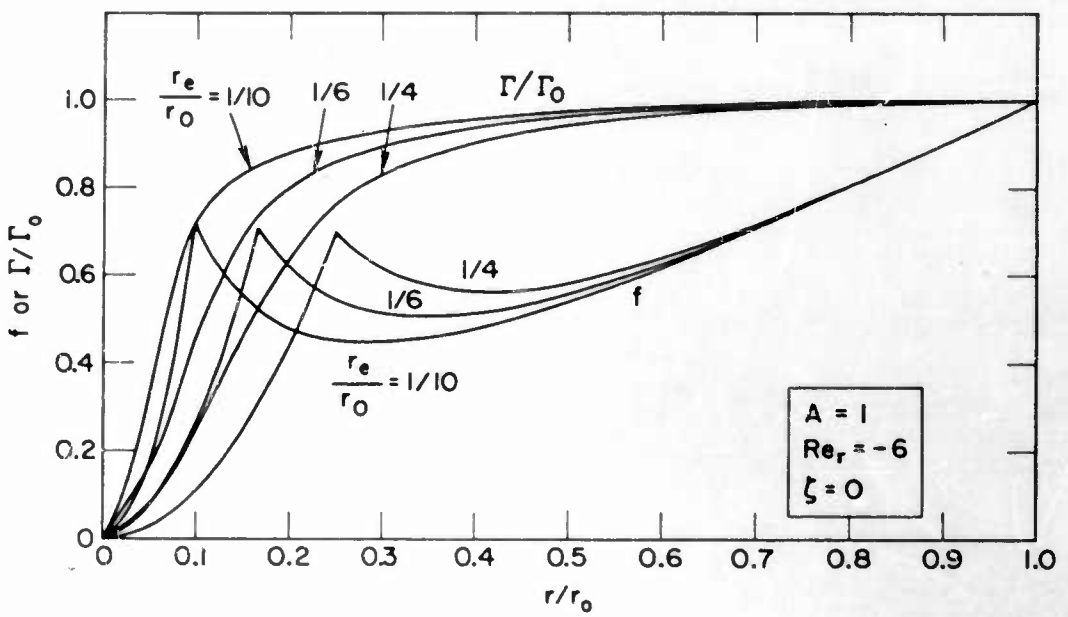

Fig. 16. Circulation and Stream Function Distributions as a Function of Radius for A = 1, ζ = 0, Re_r = -6, and Various Values of r_e/r_0

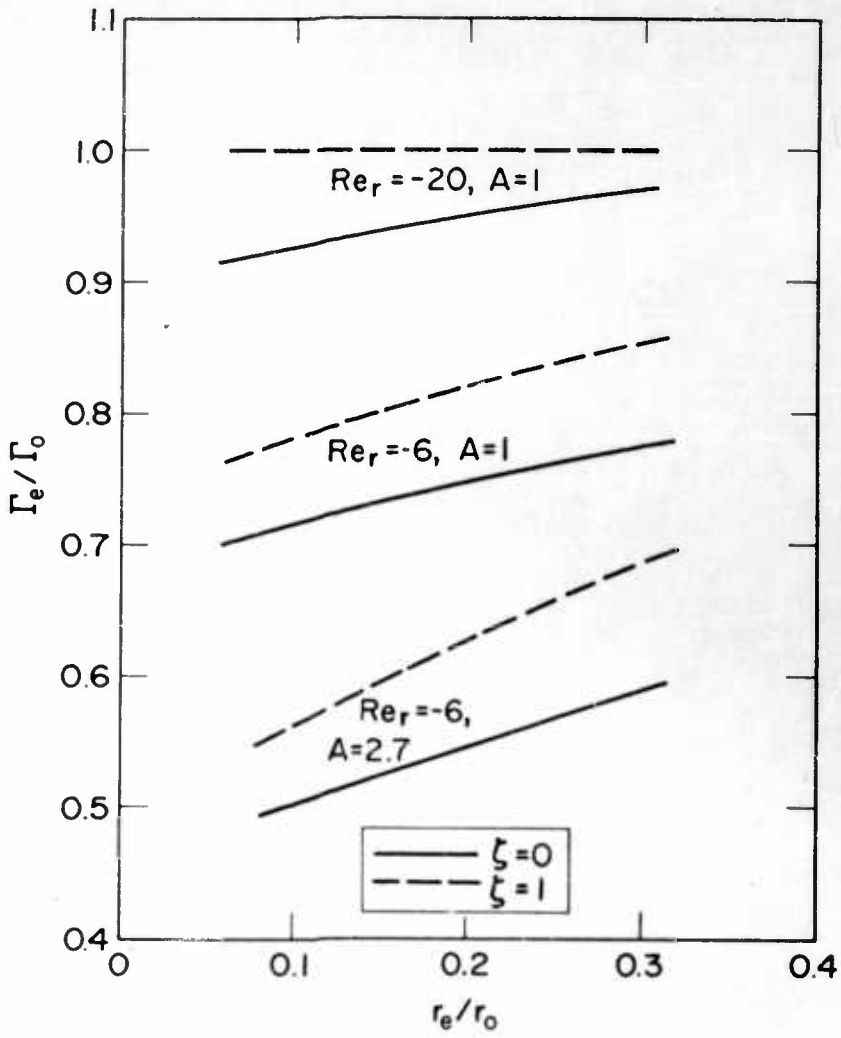

Fig. 17. Circulation at the Edge of the Exhaust Radius as a Function of the Exhaust Radius

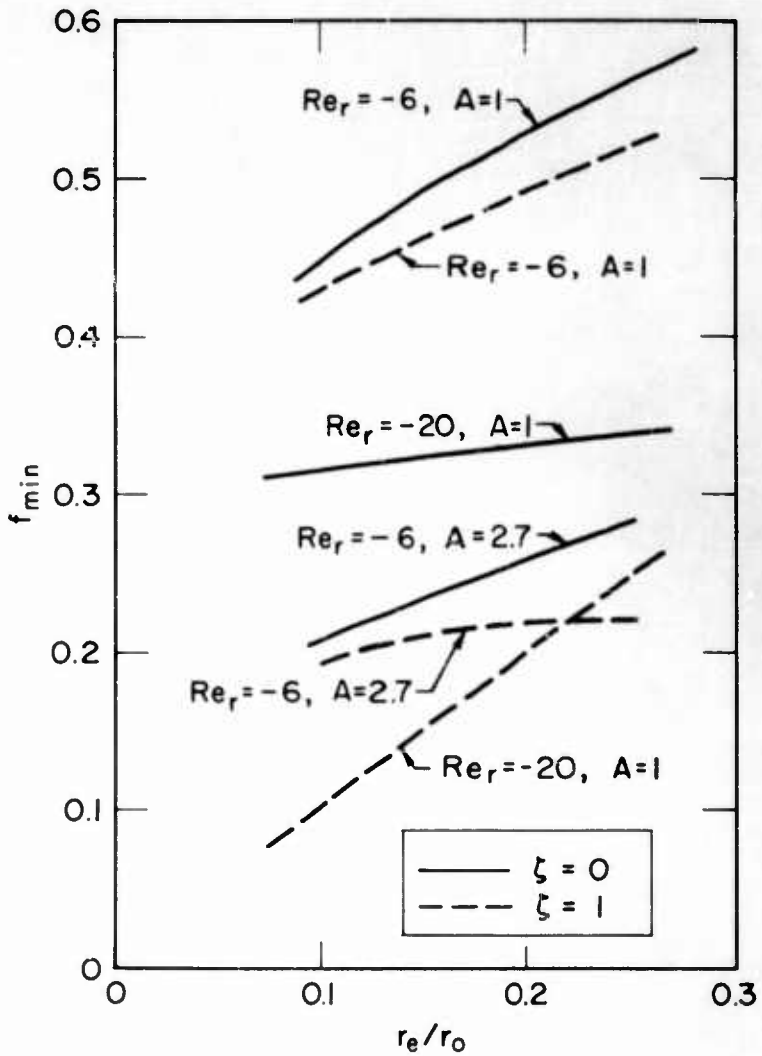

Fig. 18. Minimum Mass Flow in the Primary Flow as a Function of the Exhaust Radius

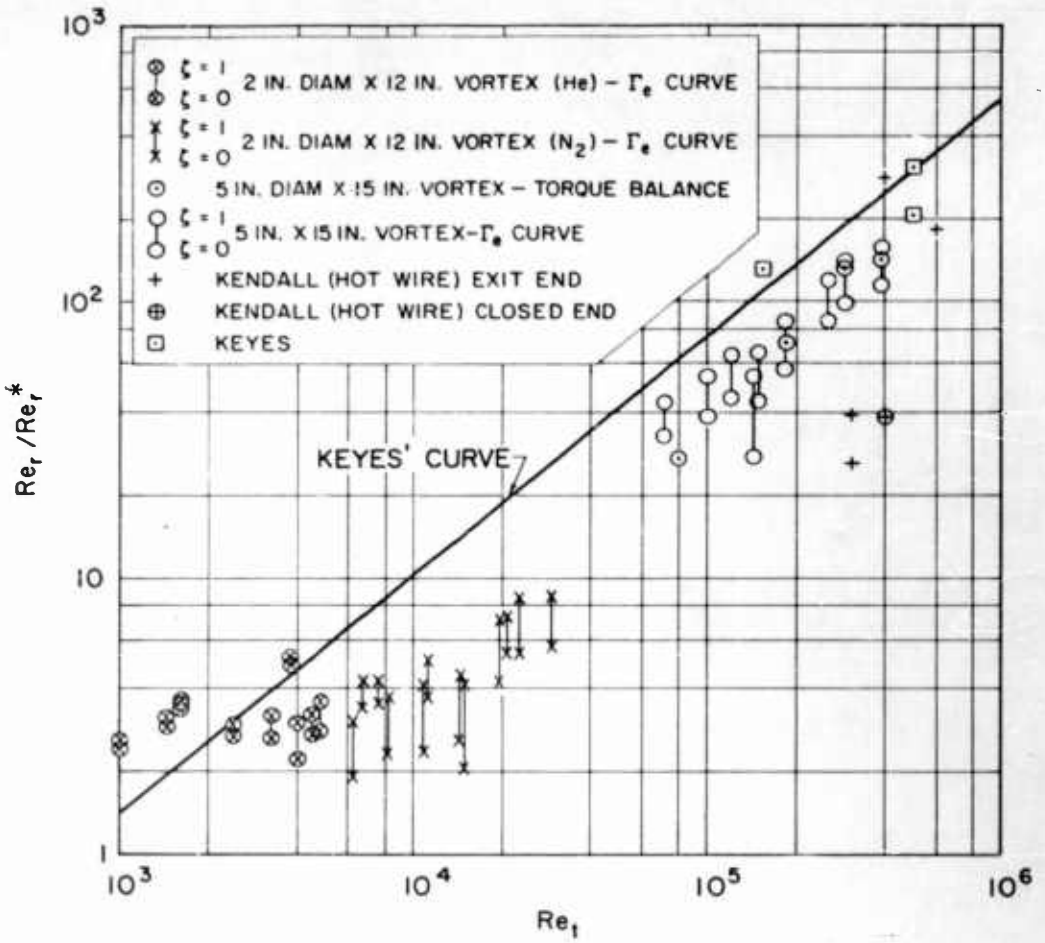

Fig. 19. The Ratio of Laminar Radial Reynolds Number to Effective Turbulent Radial Reynolds Number as a Function of Tangential Reynolds Number

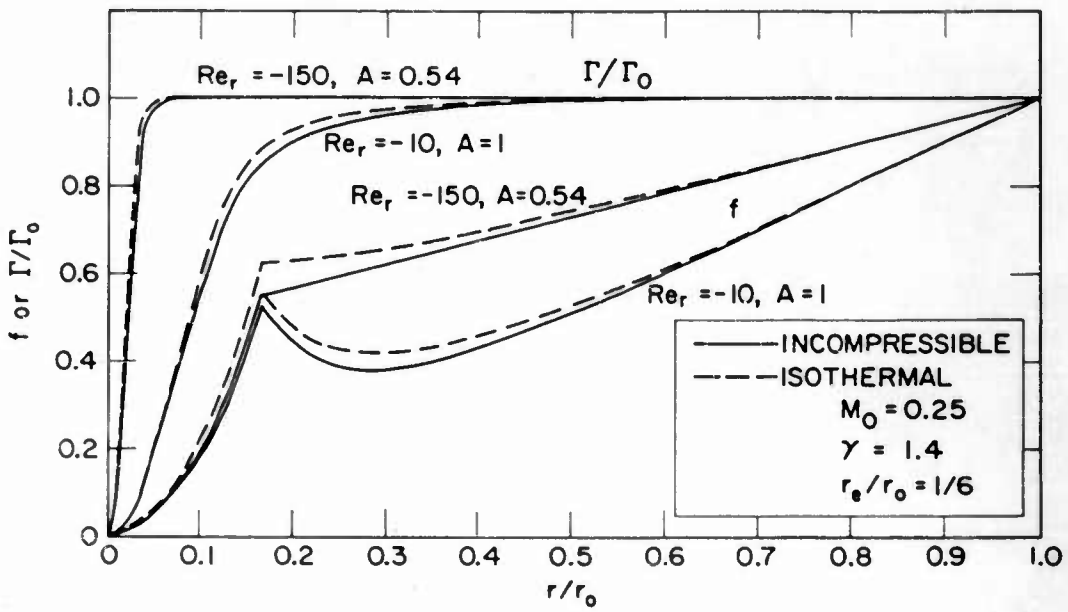

Fig. B-1. Circulation and Stream Function Distributions as a Function of Radius Showing the Effect of Compressibility for $M_0 = 0.25$